Review Vol. 13, No. 11 / 1 Nov 2023 / Optical Materials Express 3068
Optical Materials EXPRESS

Near-field imaging and spectroscopy of terahertz resonators and metasurfaces [Invited]

LUCY L. HALE,[1,2,†] THOMAS SIDAY,[1,3,†] AND OLEG MITROFANOV[1,*]

[1]Electronic and Electrical Engineering, University College London, Torrington Place, London, WC1E 7JE, UK
[2]present address: ETH Zurich, Institute of Quantum Electronics, Auguste-Piccard-Hof 1, 8093 Zurich, Switzerland
[3]present address: Department of Physics, University of Oxford, Oxford OX1 3PU, UK
[†]These authors contributed equally to this work.
[*]o.mitrofanov@ucl.ac.uk

Abstract: Terahertz (THz) metasurfaces have become a key platform for engineering light-matter interaction at THz frequencies. They have evolved from simple metallic resonator arrays into tunable and programmable devices, displaying ultrafast modulation rates and incorporating emerging quantum materials. The electrodynamics which govern metasurface operation can only be directly revealed at the scale of subwavelength individual metasurface elements, through sampling their evanescent fields. It requires near-field spectroscopy and imaging techniques to overcome the diffraction limit and provide spatial resolution down to the nanoscale. Through a series of case studies, this review provides an in-depth overview of recently developed THz near-field microscopy capabilities for research on metamaterials.

1. Introduction

At terahertz (THz) frequencies, the interaction of solid materials with electromagnetic waves is primarily determined by free electrons and bound atomic charges. The response of free electrons varies with their density, mobility and the number of degrees of freedom, whereas the response of atomic charges in crystalline materials is governed by the crystal lattice structure, which can exhibit vibrational modes (phonons) in the THz range [1–3]. Engineering a desired material response at THz frequencies only with the help of mechanisms which naturally occur in materials however is highly restrictive. In contrast, the concept of metamaterials and metasurfaces provides an incredibly flexible approach to tailoring light-matter interaction with frequency selectivity [4–7]. Owing to the large wavelength of THz radiation, fabrication of THz metasurfaces can be realized with standard semiconductor fabrication processes, and development of artificial THz materials has been steadily growing over the past two decades [6,8–10]. Furthermore, metamaterials concepts have been applied in active devices [8,11], enabling THz modulators [12], sensors [13], and emitters [14–16]. Future THz devices will undoubtedly include THz metasurfaces and metamaterials for controlling and manipulating THz waves, such as flat lenses [17], generators of complex THz beams [18], waveguides [19–21] and detectors [22].

The functionalities and performance of THz metamaterials originate from a sub-wavelength size element that can support resonances at THz frequencies. Much of the development in recent years has been focused on design and experimental verification of such resonators or "meta-atoms," through which THz properties can be engineered. So far, numerical electromagnetic modelling has served as the main tool for designing THz resonators and metasurfaces. While experimental spectroscopy techniques, such as Fourier transform infrared (FTIR) spectroscopy

#502318 https://doi.org/10.1364/OME.502318
Journal © 2023 Received 2 Aug 2023; revised 15 Sep 2023; accepted 15 Sep 2023; published 3 Oct 2023

Optical Materials EXPRESS

and THz time-domain spectroscopy (TDS) are now well established, they rarely possess the sensitivity to investigate single resonators due to very small overall extinction values for a single element [23–27]. Arrays of resonators are therefore typically investigated instead, even though inter-resonator coupling can significantly affect the array response in comparison to isolated resonators [26,27]. More importantly, internal mechanisms operating within individual resonators, as well as in metasurfaces, remain obscured in the far-field measurements, because resonant fields are typically subwavelength in nature and the interaction between resonators primarily occurs through evanescent fields, which cannot be sampled in the far-field.

The technical problem of revealing the internal working mechanisms in resonators becomes even more challenging for resonators made of less understood emerging materials [28]. Even established semiconductor structures with unknown doping levels and unknown carrier distribution within the structure volume present challenges for accurate modelling [24,29]. What is required to address these research challenges is a method for probing THz evanescent fields near resonators and metasurfaces, which can reveal the nature and properties of supported resonances, alongside mechanisms of inter-resonator coupling. It could also aid in characterization of more complex photonic states, including the corner and edge states [20], bound-in-the-continuum states [30], dark modes and photonic modes with large wavevectors.

Near-field microscopy and near-field spectroscopy provide such capabilities. Developed originally for optical, infrared and microwaves parts of the electromagnetic spectrum [31–33], these techniques were adapted for the THz frequency range and have become more widely used in recent years. However, the enormous span of length scales needed for THz analysis (from diffraction limit to the nanoscale) and special instrumentation required for generation and detection of THz waves also prompted development of specialized THz near-field microscopy approaches. Currently, however, no single approach can cover the entire span of length scales and provide all the developed functionalities, which include mapping of the electric field vectorial components, detection of transient field evolution and controlled launching of surface plasmons. Instead, these THz near-field microscopy and spectroscopy methods now form a suite of tools with unique capabilities.

In this Article, we provide a brief review of recently developed THz near-field microscopy and spectroscopy methods for revealing the internal physical mechanisms at work in THz resonators and metasurfaces, and highlight some of the unique capabilities that near-field techniques provide. We start with a brief description of fundamental properties of sub-wavelength THz resonators and confined electromagnetic fields (Section 2), then we overview the major near-field microscopy approaches (Section 3), and finally illustrate their applications and their remarkable capabilities using examples from the literature (Section 4).

2. Subwavelength THz resonators

2.1. THz resonators

The fundamental building block in THz metamaterials is an electromagnetic THz resonator. Simple examples of resonators are a high-permittivity spherical particle [34] or a conductive element in a shape of a dipole antenna or a split ring [35]. At THz frequencies, conductive resonators made of metals or semiconductors have been extensively used to build metasurfaces and metamaterials [6,8–10,29]. Their properties are controlled through the resonator geometry. Conductive resonators can easily enhance and concentrate the electric field of an incident wave in a desired spatial region, and change the electric field orientation, enhancing light-matter interaction and enabling a number of practical THz devices [12]. Dielectric THz resonators have also shown promise because of readily available materials with relatively large dielectric permittivity and small losses, such as silicon ($\varepsilon_r \sim 12$) [36]. Higher permittivity materials, including TiO_2 ($\varepsilon_r \sim 100$) [23,37], can increase the quality factor of resonators and reduce their geometrical size. Beyond standard metals and dielectrics, several material systems including graphene

Optical Materials EXPRESS

and other 2D van der Waals materials [38–42], topological insulators [43–47], semimetals [48] and superconductors [49,50] are currently actively investigated for applications at THz frequencies. These material systems can expand the functionalities of classical THz resonators, promising deeply sub-wavelength designs (< λ/10), tunability, strong field confinement and field enhancement.

All resonators described above are subwavelength in nature, and experimental characterization of their properties is challenging. To understand the fundamental principles of subwavelength resonators and gain insight into challenges in probing their properties, here we consider two simplest examples of THz resonators illustrated in Fig. 1(a) and 1(b).

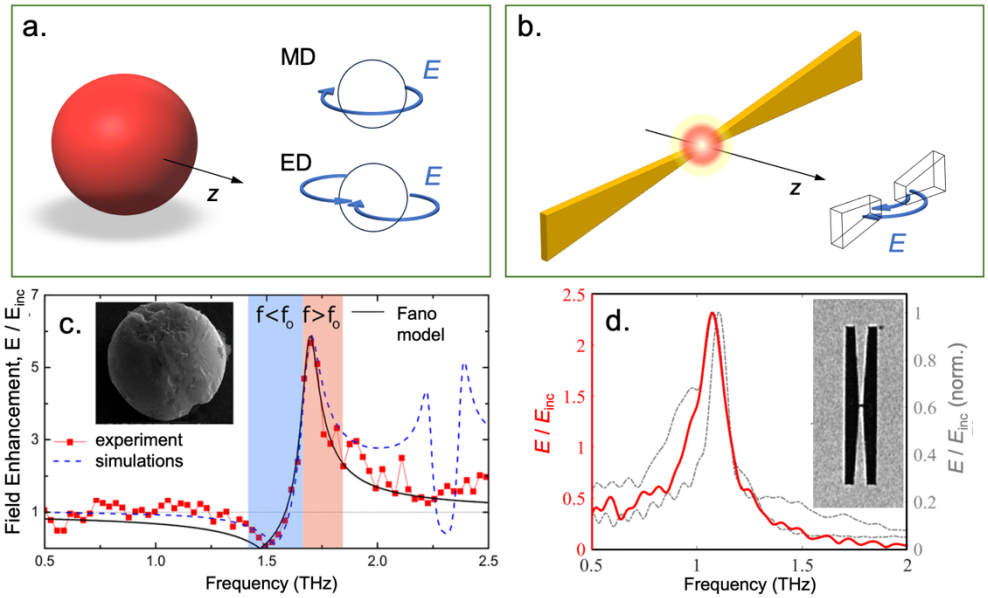

Fig. 1. Basic THz resonators and their spectra: **a.** High dielectric permittivity sphere supporting the magnetic dipole (MD) and electric dipole (ED) modes with an illustration of corresponding electric field lines outside the sphere; **b.** Plasmonic resonator consisting of two dipole antennas with a small gap between their tips; **c.** Electric field spectrum (normalized to the incident field spectrum) near an anisotropic TiO_2 sphere of radius $r = 10.7$ μm: experiment (red symbols) measured by aperture-type THz near-field microscopy, numerical simulations (blue dashed line) and a Fano lineshape fit (black line) (adapted from [37] © 2016 Wiley-VCH); **d.** Electric field spectrum (normalized to the incident field spectrum) near the gap of a complementary LC resonator with an integrated tapered dipole antenna in the center (the length of the resonator is 50 μm): red line shows the field amplitude spectrum for a single resonator, and dashed and dotted lines show spectra for arrays of such resonators with two different periods (adapted from [26] © 2020 Wiley-VCH [26]).

A dielectric sphere with permittivity significantly larger than the environment supports Mie modes with strong fields in the sphere (Fig. 1(a)) [34]. These modes are not bound within the sphere, and they can therefore be excited by an incident plane wave, displaying peaks in absorption and scattering cross-section spectra (Fig. 1(c)) [34]. At the resonance frequencies, optical fields inside the sphere can be several times stronger than the field of the incident wave, similar to a standing wave formed in a cavity with a transparent boundary.

For a sphere made of a large dielectric permittivity material, the two lowest order modes are the magnetic dipole (MD) and electric dipole (ED) modes, and they are characterized by the free-space wavelength several times larger than the sphere diameter. As a result, the

Optical Materials EXPRESS

electromagnetic field energy can be concentrated in a volume much smaller than the free-space wavelength. For illustration, a 20 μm in diameter TiO_2 sphere supports MD and ED modes with corresponding free space wavelengths of ~175 μm (1.7 THz) and ~130 μm (2.3 THz) respectively [23,37].

Even stronger field confinement can be achieved in a plasmonic resonator. In an example shown in Fig. 1(b), a resonator consists of two tapered dipole antennas with a small capacitive gap between the antenna tips, which confine the incident field to a deeply subwavelength volume. To capture the energy of an incident THz wave efficiently, the dipole antenna length is designed to be approximately ½ of the wavelength.

THz spectroscopy performed in the near-field zone of such resonators has provided direct experimental characterization of the localized fields and revealed their spectra [23,26,37]. Figures 1(c) and 1(d) show THz spectra measured by aperture THz near-field microscopy at the surface of a TiO_2 spherical resonator [37] and near the capacitive gap of a complementary LC resonator [26]. In both cases, the experimental spectra (normalized to the incident THz pulse spectrum) clearly show resonances as enhancement of the detected electric field within relatively narrow bands of frequencies.

2.2. Subwavelength field confinement and representation in momentum space

Both dielectric and plasmonic resonators display enhanced localized electric fields at resonance frequencies. However, these fields decay within a short (subwavelength) distance from the surface, and therefore they present challenges for detection with far-field spectroscopy techniques [23,27,47]. In fact, all fields confined to a subwavelength volume are largely non-radiative. To understand the physics behind this effect, it is informative to represent the spatial field distribution for the confined wave as a superposition of plane waves in the momentum (k-vector) space.

We can illustrate this by considering a THz wave travelling between two sharp metallic needles commonly used in scanning tunnelling microscopy (STM). As the THz wave travels along the needles, it will induce charges along their surface, allowing the field lines to terminate at the needles' surfaces. As the distance between the needles decreases toward their tips, they will start confining the THz wave to a small deeply subwavelength volume. Figure 2(a) shows an example of experimentally mapped distribution of THz electric field $E_x(x,y)$ near the needles' tips [51]. The THz field is confined to an area of only a few micrometers across (note that the entire image in Fig. 2(a) is smaller than the THz wavelength).

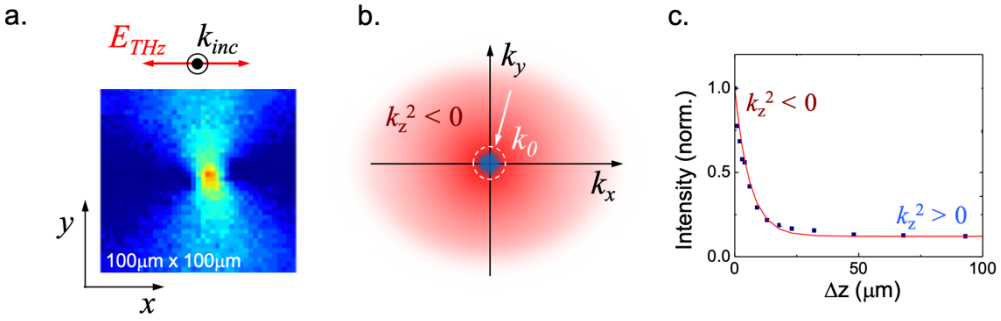

Fig. 2. Illustration of confined THz fields and their k-vector spectrum: **a.** THz electric field distribution at the tips of two sharp metallic needles mapped by aperture-type THz near-field microscopy (adapted with permission from [51] © 2012 The Optical Society [51]); **b.** Schematic illustration of the corresponding spatial frequency spectrum (in the momentum space); **c.** THz field intensity measured as a function of distance from the tips along the z-axis (adapted from [51] © 2012 The Optical Society).

Optical Materials EXPRESS

In Fig. 2(b) we schematically illustrate a 2D Fourier transform spectrum $E_x(k_x,k_y)$ of the real-space distribution in Fig. 2(a). Most of the spatial frequencies in the spectrum are characterized by the in-plane k-vector with the absolute value $| k | = (k_x^2 + k_y^2)^{1/2}$ larger than the THz k-vector in free space, $k_0 = 2\pi/\lambda$. The white dashed circle in the k-space diagram separates two regions, where the spatial frequencies are either smaller or larger than k_0. For a strongly confined field distribution, such as the one in Fig. 2(a), most of its energy will be in the k-vector components outside the circle. These spectral components cannot continue propagating in the z-direction as they are characterized by purely imaginary k_z values: $k_z = (k_0^2 - k_x^2 - k_y^2)^{1/2}$. Indeed, the highly confined field near the tips quickly decays with distance from the tips. The decay is illustrated in the experimental plot of THz field intensity measured along the z-axis (Fig. 2(c)) [51].

Similarly, non-radiative (evanescent) k-vector components of the fields concentrated by a resonator decay exponentially with distance from it, and only a small fraction of the energy in the confined fields leaks as propagating waves to the far-field zone, carrying information about its resonant properties. This poor coupling of strongly confined resonant fields to free-space propagating waves makes investigation of single subwavelength resonators difficult using far-field techniques. Moreover, the key information about the modes, such as their spatial profiles, is lost in the far-field. In contrast, near-field THz imaging and spectroscopy methods are ideally suited for spatial mapping of the localized fields and analyzing their spectra.

3. THz near-field imaging and spectroscopy methods

First demonstrations of THz imaging with sub-wavelength spatial resolution followed promptly after the development of THz time-domain spectroscopy and imaging [52–54]. Such a rapid progress was driven by the need for THz characterization with spatial resolution better than the diffraction limit. Over the years, the field of THz near-field imaging and spectroscopy has evolved into a scientifically rich and active research area and several advanced techniques have been developed simultaneously, pushing the spatial resolution from the diffraction limit first down below 10 μm [55,56], and later to 10s of nanometers [57–59]. These techniques now cover length scales spanning approximately five orders of magnitude. THz resonators and metasurfaces fall into a region of the application space, where several techniques can be successfully utilized [60].

Selecting an appropriate technique however requires good understanding of what each approach can provide and where limitations lie. While some investigations may require sub-micron spatial resolution, for example studies of surface plasmon resonances in topological insulators [45,46], other investigations may need the sensitivity to modes confined below the resonator surface [25], or may focus on inter-resonator coupling for bound-in-continuum (BIC) modes extended over lengths of millimeters [30]. To understand the advantages and drawbacks of different techniques for characterization of THz resonators and metamaterials, in this section we briefly overview major THz near-field imaging and spectroscopy approaches, their operation principles and their unique capabilities.

The first THz near-field imaging demonstration followed one of the classical near-field microscopy schemes [31] and employed a subwavelength aperture (~λ/10) in the tip of a metallic cone serving as a subwavelength-size THz pulse source [54]. A sample was illuminated through the aperture and a transmitted THz wave was detected in the far-field using a THz time-domain spectroscopy (TDS) system. By raster-scanning an object with respect to the aperture, a THz image was constructed with a spatial resolution defined by the aperture size, rather than the wavelength. While this approach overcame the diffraction limit, it also showed severe attenuation of the transmitted THz wave. Further reduction of the aperture size was impractical in that configuration [55].

To mitigate the problem of strongly suppressed transmission through a deeply subwavelength aperture [55], a different configuration, known as the collection mode near-field microscopy, was developed [61]. In this configuration, the entire sample was illuminated uniformly, whereas a

Optical Materials EXPRESS

near-field probe with an aperture was used to sample the THz field locally [61]. With advances in the near-field probe design, this configuration later pushed the spatial resolution of aperture-type THz microscopy and THz time-domain spectroscopy analysis to ~2 μm [62,63].

In parallel, rapid development of THz detectors with subwavelength-size sensing elements have opened doors to a class of THz near-field probes which can be introduced directly into the evanescent field region and detect local THz electric fields without an aperture, enabling local THz spectroscopy and subwavelength resolution imaging. Among such detectors are micrometer-scale electro-optic (EO) probes [64–67] and micro-fabricated THz photoconductive detectors [68]. Spatial resolutions in the range of 5-10 μm have been demonstrated with these techniques [67], limited only by the size of THz detectors and their sensitivity. Despite the limitations these approaches have enabled direct probing of vector components of THz fields [68] and video-rate near-field THz imaging [67].

The highest spatial resolution among THz near-field methods (excluding THz-STM methods, which rely on ultrafast tunneling currents for spatial resolution [60,69]) can be provided by scattering THz near-field microscopy (commonly known as scattering-type Scanning Near-field Optical Microscopy, s-SNOM) [70]. This method is based on the platform of atomic force microscope (AFM), it can be used with a number of different light sources, and in addition to THz imaging it also provides topographical images. The first experimental demonstration of s-SNOM in the THz frequency range was also reported in the early years of THz near-field microscopy research [57]. However, it took several years before the s-SNOM technique became more widely used in the THz range [28,40,41,45,46,48,58,70–80]. Scattering of the THz waves by an AFM probe is weaker in comparison to the optical and near-IR waves by orders of magnitude. The difficulty of acquiring sufficiently strong s-SNOM signals prompted development of special THz near-field probes with enhanced scattering efficiency [59,72–74,81], which have pushed the limit of spatial resolution down to 10-20 nm (~λ/10,000) [59].

While spatial resolution is one of the main capabilities enabled by the near-field microscopy methods, all the techniques mentioned above display their unique interaction with the sample, leading to unique imaging features. The direct detection near-field microscopy, including the aperture-type, EO and micro-probes, tends to produce images that correlate with the electric field distribution in the sample, whereas the THz-s-SNOM signal contrast correlates with a combination of the THz field and a value of local sample permittivity at THz frequencies. Another aspect of near-field microscopy that must be emphasized is the influence of near-field probe on the measurements. It is commonly recognized that evaluation of the probe influence is an integral part of near-field image analysis, and several important probe-sample interaction mechanisms have been identified and studied over the years [40,45,46,82]. Interestingly, some of these mechanisms allowed researchers to drastically expand the capabilities of near-field microscopy [40,45,46] and we will discuss such examples below.

As a last comment in this brief overview, we note that a growing number of THz imaging methods have been developed over the years or are currently being actively developed [60,83]. It is beyond the scope of this review to discuss all subwavelength resolution methods. Here, we will focus only on the techniques that have been successfully applied for studying THz resonators, metamaterials and metasurfaces and revealing their internal mechanisms.

3.1. Aperture-type THz near-field microscopy and spectroscopy

Aperture-type THz near-field microscopy and spectroscopy provide methods for mapping the electric fields in the sample vicinity and performing local THz spectroscopy at a desired location. The aperture approach has been applied to investigate a wide range of structures supporting THz resonances, including dielectric spherical resonators [23], metallic plasmonic resonators [24,84], resonators made of topological insulators [47] and graphene [39], as well as more complex

Optical Materials EXPRESS

plasmonic resonators supporting dark (non-radiative) modes [25,85]. Examples of THz near-field spectra for a plasmonic and dielectric resonator are illustrated in Fig. 1.

In a typical aperture microscopy setup, a single THz resonator is illuminated at normal incidence by a THz beam from the substrate side, while a near-field probe (P) with a small input aperture (A) is positioned near the resonator (typically at ~5 μm from the resonator surface) as illustrated schematically in Fig. 3(a). In response to the incident wave, resonant THz fields are formed near the resonator. When the aperture probe is introduced in the evanescent field region, these resonant fields can couple through the aperture in the metallic screen to be detected on the other side of the screen by a THz detector (D), for example a photoconductive antenna (PCA).

The inset of Fig. 3(a) illustrates results of THz mapping with an aperture probe. Standing wave patterns were visible on a carbon fiber excited by a THz pulse. Two images show 'snapshots' of the THz field mapped with a time interval of ~0.27 ps [63]. During that interval, the phase of the detected wave changes by π, indicating resonant oscillations at a frequency of ~1.85 THz [63].

The aperture-type probe can be also used for local THz-TDS analysis. The probe detects not only the localized fields, but also the incident THz wave used to excite the resonator. Measurements of the incident wave provides a reference for normalizing the local field spectrum to the incident field spectrum, similar to the far-field THz-TDS analysis. This normalization procedure eliminates the frequency-dependent sensitivities of the probe and the detector from the analysis and provides spectra of the local fields independent of spectral content of the THz source. For illustration, in the inset of Fig. 3(a), the spatial field distributions showed mainly the 3λ/2 dipolar mode. However, near-field THz-TDS analysis on this sample not only showed a spectral peak corresponding to 3λ/2 mode, but also revealed a λ/2 resonance, which is not visible in the space map due to a lower spectral power density at the corresponding frequency [63]. In another study, near-field THz spectroscopy analysis revealed a set of sub-surface plasmonic modes supported by double-metal THz resonators [25].

The main limitations of aperture-type microscopy lie in the spatial resolution and probe invasiveness. Although the aperture size determines spatial resolution, transmission through a subwavelength aperture reduces quickly with the aperture size, a: the transmitted power scales as a^6 in the far-field [55]. Such a severe attenuation limits applications of stand-alone aperture probes. However, sensitivity of aperture-type THz probes was improved by orders of magnitude by integrating a THz detector into the probe within ~ 1 μm from the aperture, and apertures as small as 2 μm, with corresponding spatial resolution, have been demonstrated [63].

Detailed investigations of plasmonic and dielectric resonators showed that the invasiveness of aperture probes diminishes as the sample-probe separation is increased to 5-10 μm. However, the localized fields also decrease in amplitude with the sample-probe separation, and therefore an optimum separation that allows characterization of localized resonances with minimal invasiveness must be evaluated. In practice, this separation is ~5 μm [24,26,37]. Since the separation also limits the spatial resolution, probes with apertures of 5-10 μm are optimum for such investigations.

Aperture-type THz near-field microscopy has provided a robust method to probe and map fields of THz resonators and metamaterials. This method has been tested with a wide range of THz resonators, which includes dielectric and plasmonic resonators. Various THz detectors, including photoconductive [62], photo-thermoelectric [86,87], and SiGe-HBT-based [88] and 2DEG-based [89] detectors, have been integrated into near-field probes enabling aperture-type THz microscopy with pulsed and CW THz sources. The sensitivity of the aperture probes to surface plasmon waves has been observed in a number of studies [24–26,61,63,82,85]. Surface plasmon waves by nature are confined to the surface and therefore require special techniques for detection. In this context, the aperture-type microscopy has become particularly valuable for analysis of THz plasmonic resonators and inter-resonator coupling. It has enabled detailed characterization of

Optical Materials EXPRESS

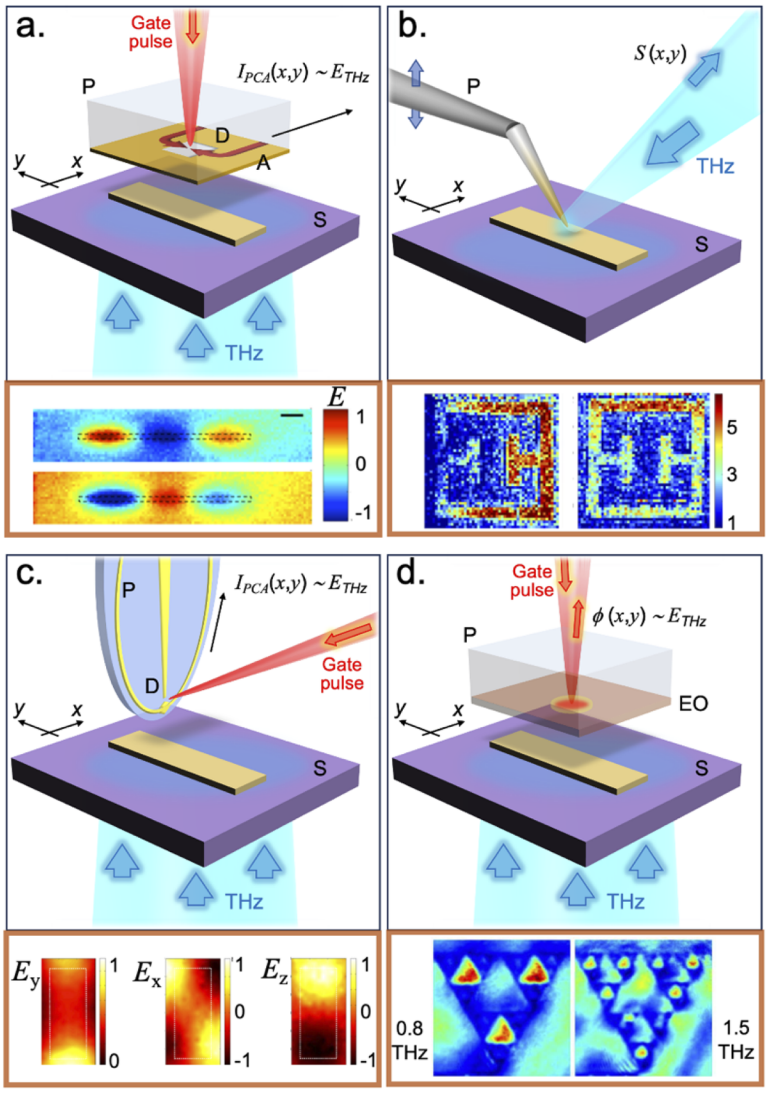

Fig. 3. Common THz near-field microscopy and spectroscopy configurations. **a.** Aperture-type THz near-field microscopy: schematic diagram illustrating excitation of a plasmonic dipole antenna resonator (S) and detection by the aperture probe (P) positioned above it. Experimental THz near-field maps showing 'snapshots' of the 3λ/2 plasmonic resonance in a carbon microfiber recorded ~1 ps after the excitation with an interval of ~0.27ps (adapted, with permission, from [63] © 2016 IEEE). **b.** Schematic illustration of scattering-type SNOM system showing the THz beam focused in the AFM probe region with the sample underneath. *Inset:* examples of THz s-SNOM near-field images of a split-ring resonator at 3.45 THz (adapted from [75], CC BY). **c.** Schematic diagram of near-field microscopy with THz micro-probes (P); *Inset:* maps of electric field components E_x, E_y and E_z near a planar metallic THz dipole antenna (adapted from [68], CC BY) **d.** Electro-optic (EO) near-field imaging: schematic diagram of a typical setup: an EO crystal is positioned close to the resonator surface and an optical probe beam is directed to the crystal. THz fields are detected through a change in the phase of the reflected beam $\phi(x,y)$. *Inset:* EO near-field images of a Sierpinski fractal antenna at two selected frequencies, showing multiple resonances arising in the structure (adapted with permission from [67] © 2016 The Optical Society [67]).

Optical Materials EXPRESS

their spectral characteristics in the single resonator regime, allowing development and refinement of advanced resonator and metasurface designs.

3.2. Scattering-type THz near-field microscopy

The scattering-type THz near-field microscopy approach uses an AFM probe (P) to scatter the evanescent waves from the surface of a sample (Fig. 3(b)). The AFM probe has a sharp, typically sub-100 nm radius metal tip, which is brought in nanometer-scale proximity with the sample. The small scatterer size and the short distance from the surface enable a nanometer-scale spatial resolution of this THz near-field microscopy approach [70]. It has been recently applied for imaging of metallic antennae [75,90] and split-ring resonators (SRR) [75,91], as well as for detection of high-momentum THz surface plasmon excitations in topological insulators [45,46], which can form the basis for nanoscale resonators.

In a typical setup (including commercially available systems), a specialized AFM probe with a sample underneath is illuminated by a focused THz beam at an incidence angle of 45-60 degrees (Fig. 3(b)). The probe-sample separation is modulated at a tapping frequency close to the mechanical resonance frequency. The scattered THz waves are then collected and sent to a THz detector (Fig. 3(b)). Due to non-linear dependence of the scattered wave amplitude on the separation, the amplitude varies at the tapping frequency, as well as at the higher harmonics. The signal is then demodulated at one of the harmonics to take advantage of the nonlinearity and extract the near-field signal from the far-field scattered waves.

The inset of Fig. 3(b) shows THz s-SNOM maps recently recorded by raster-scanning a metallic SRR with respect to the AFM tip [75]. The outline of the metallic resonator on a dielectric substrate is clearly seen in the near-field THz image. In addition, the signal strength varies for the opposite sides of the SRR when the incident wave matches the resonance frequencies. The images are also sensitive to the resonator orientation: in the left image, two capacitive elements of the SRR show enhanced THz signal, whereas the opposite sides of the outer ring show contrast in the right image, where the SRR was rotated 90 degrees around its center [75]. These results demonstrate the ability of s-SNOM to detect two quantities: material permittivity at THz frequencies and the field of surface plasmon excitation. The former is useful for mapping the THz material properties (dielectric function) with very high spatial resolution, for example for characterizing local conductivity or the local doping density [92].

This ‘material’ contribution to the s-SNOM signal is often dominant and it interferes with the evanescent fields of resonator modes, causing complications in the image analysis. Nevertheless, these contributions often can be separated through control of the incident beam polarization, sample orientation, and through analysis of simultaneously recoded amplitude and phase of the scattered signal. Additional complications, e.g. asymmetry in the near-field images, can be caused by the oblique illumination geometry leading to phase retardation effects in this near-field configuration [91]. Furthermore, the probe itself can act as an antenna and can modify the scattered field efficiency on the opposite sides of the resonator [91]. Recently, it was found that s-SNOM probe itself can launch THz surface plasmons [93,94]. While the tip-launched surface plasmon affect near-field images, they have been used effectively for characterizing surface plasmons in novel materials [40,41,45,46].

The interaction between the tip apex and sample and the requisite modulation of tip-sample separation in s-SNOM complicates quantitative extraction of material properties, and several analytical models for describing the scattering process have been developed to address this. The point- and finite-dipole models [32,95,96] have become commonplace at mid-IR frequencies [70]. More recently, these analytical scattering models have also been applied at THz frequencies, demonstrating reasonable qualitative agreement with experimental results [58,76,77,79]. However, at THz frequencies the macroscopic geometry of the probe plays a far more prominent role in the scattering process [72,73,78–80]. This has prompted a significant interest in solving

Optical Materials EXPRESS

the scattering problem numerically [28,80,81], although such simulations are computationally intensive and often impractical for everyday use.

THz-s-SNOM investigations, and particularly studies of THz resonators and metamaterials, are still relatively rare, despite exhaustive developments of this technique in the IR range [70]. THz-s-SNOM studies of resonators remain challenging due to the complex nature of the scattered signal, phase retardation effects and the impact of the near-field probe geometry. Nevertheless, the nanoscale spatial resolution and the effect of surface plasmon launching by the tip offer unique opportunities to reveal and investigate highly confined THz surface plasmon-polaritons in emerging materials, thus providing key characteristics needed for utilizing these materials in photonics applications, including THz metasurfaces.

3.3. THz photoconductive micro-probes for near-field microscopy and spectroscopy

Direct detection of THz fields in the near-field zone without invasiveness of a near-field probe or without contact with the sample surface is the ultimate characterization capability needed for development of THz metasurfaces and metamaterials. Electromagnetic fields are presently extracted from numerical simulations, and they are routinely used in design of metasurfaces. Accessing details of the electromagnetic fields experimentally would close the design loop and allow refining material models, especially needed for emerging materials.

Direct probing of confined THz fields is possible thanks to the relatively large size of THz resonators and advances in compact THz detectors, although demonstrations are still rare. Among technologies that showed direct electric field mapping are THz micro-probes with photoconductive detectors (Fig. 3(c)) [68]. They have expanded the near-field mapping capabilities by providing full vectorial mapping of THz fields and their evolution.

The THz micro-probes contain photoconductive switches as illustrated in Fig. 3(c). They are designed to detect only selected components of the complex THz electric field vector without significant crosstalk [68]. The probes can be freely positioned in three dimensions and can be introduced into the evanescent field region within several micrometers from a sample surface with minimal invasiveness. The inset of Fig. 3(c) illustrates results of electric field component mapping for a planar THz dipole antenna [68]. The antenna was excited by a weakly focused THz beam, and the THz fields were mapped using two types of micro-probes: one detecting the out-of-plane electric field (normal to the surface) and the other detecting the in-plane THz field, with the photoconductive antenna gap orientation determining a specific in-plane field direction [68].

The THz field detection principle and mechanism used in these probes are the same as in conventional photoconductive THz detectors used in THz-TDS systems. They therefore provide not only the full vectorial fields, but also can be used for local coherent THz spectroscopy and for visualizing evolution of THz electric fields within a resonator or a metasurface. Spatial resolution provided by the micro-probes is in the range of several micrometers and it is sufficient for investigating many THz resonators and metasurfaces.

3.4. Electro-optic THz near-field microscopy

EO THz near-field imaging has been recognized as one technology that can provide video-rate 2D mapping of THz fields in the near-field without sample scanning [53]. It can be realized by introducing a thin EO crystal in close proximity to the sample surface where resonant THz fields are present, as illustrated in Fig. 3(d) [67]. The EO effect in the crystal modifies the refractive index proportionally to the THz field strength, and this change is then imaged using an optical probing beam. After reflection from the bottom side of the crystal, the probe beam is projected through a polarizer-analyzer onto a camera, and a near-field map of the entire sample is imaged without scanning.

Optical Materials EXPRESS

The inset of Fig. 3(d) illustrates EO near-field images of a Sierpinski fractal antenna, which is composed of triangular resonators of various sizes [67]. The images show multiple resonances arising in the structure as they produce field enhancement in corresponding resonators. Spatial resolution in EO THz near-field microscopy is limited by the resolution of the optical imaging system (typically 5-10 μm) and the thickness of EO crystal. The example in the inset of Fig. 3(d) shows one of highest spatial resolutions achieved using this approach. It was realized with the help of a 1-μm-thick *x*-cut lithium niobate crystal attached to a glass substrate (the antenna was directly patterned onto the crystal) [67].

As in the other near-field approaches, invasiveness of the sensing element is a limitation of EO near-field imaging: large dielectric permittivity of EO crystals tends to modify the intrinsic fields of resonators, and it can lead to a shift in the resonance frequencies. Nevertheless, the ability to produce video-rate THz near-field images without scanning have opened doors to investigations of large area samples while providing micrometer-level spatial resolution.

4. Near-field probing of THz photonic states

Over the years, THz near-field microscopy proved to be an invaluable approach for characterization of localized fields in THz resonators and metasurfaces. Several powerful methodologies been developed and demonstrated. They can reveal surface plasmon-polariton waves and resonances, subsurface modes, components of the electric field vector and inter-resonator coupling, enable local THz spectroscopy and map mode profiles with sub-micron resolution and over the scale of many wavelengths. In this section, we highlight several powerful capabilities developed with THz near-field imaging and spectroscopy techniques.

4.1. Ultrafast evolution of local fields

One of the unique capabilities of THz near-field methods comes from combining the access to spatial distribution of THz fields with time-domain measurements and short impulse excitation. It enables visualization of ultrafast dynamics of local THz fields. The full information in space and time provides invaluable insight into the physical processes occurring in the resonators and metasurfaces. In this subsection, we describe the process of THz surface plasmon excitation in resonators revealed by near-field investigations.

We illustrate it using the carbon fiber example in Fig. 3(a), where an aperture-type near-field system was used to detect a standing wave with three crests along the fiber length [63]. These standing wave maps were recorded about 1 ps after the excitation by a THz pulse, when the resonance along the fiber has already formed. An insight into how it developed can be gained when considering prior evolution of the fields.

The field dynamics can be visualized in space-time maps of the THz field along and perpendicular to the fiber axis (Fig. 4(a)) [63]. Along the fiber axis, the map shows that the fiber initially blocks the THz wave from reaching the aperture: while the incident THz pulse is visible in the areas away from the fiber, the THz field along the fiber is delayed. At the fiber center, the delay is the longest, approximately 0.5 ps, and it gradually decreases to 0 at the fiber tips (note that in this aperture-type microscopy configuration the THz wave illuminates the sample at normal incidence).

This wavefront pattern in the space-time map measured along the fiber has the distinctive signature of a wave propagating along the fiber surface [24,63], and the delay observed at the fiber center simply corresponds to the time the surface wave travels from the fiber tips to the center. The space-time map for a line scan perpendicular to the fiber axis shows that the delayed THz fields remain localized along the fiber even after the excitation. Similar space-time field patterns were detected on metallic surfaces due to the excitation of THz surfaces waves [84]. However, unlike THz surface waves on metals, the velocity of propagation along the carbon fiber, which can be estimated directly from the space-time map using the slope of the wave pattern ($v = \Delta x/\Delta t$)

Optical Materials EXPRESS

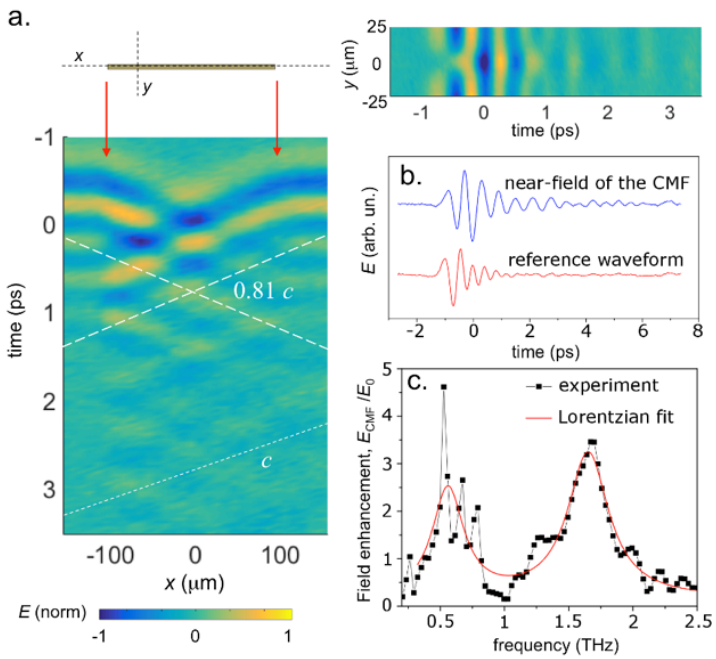

Fig. 4. Illustration of field evolution near a plasmonic resonator (207-μm-long carbon microfiber (CMF)) revealed by aperture-type THz near-field microscopy. **a.** Space-time maps of the THz field recorded along and perpendicular to the fiber axis (scan locations are shown in the schematic diagram; red arrows indicate the position of fiber tips in the map). **b.** THz time-domain waveform at the wave crest on the left side of the fiber and the reference THz pulse waveform detected at y = −30 μm. **c.** Fourier transform spectrum at the left-side crest of the standing wave normalized to the reference waveform spectrum (adapted, with permission, from [63] © 2016 IEEE).

was ~20% lower. The detected change in the phase velocity can be attributed to two factors: a reduced conductivity along the fiber in comparison to metals, and a reduced surface plasmon phase velocity due to the presence of a thin dielectric membrane supporting the fiber [24,63].

The observed evolution of local fields reveals the plasmon excitation mechanism. First, the electric field of the THz pulse drives charge carriers toward the fiber tips, polarizing the fiber and forming strongly localized fields at the tips (on the scale much smaller than the wavelength). As in the case of the THz fields localized by the STM tips in Fig. 2, the corresponding spectrum of spatial frequencies is very broad, and it includes waves with the k-vector matching the k-vector of surface plasmons. Therefore, the strongly localized field regions at the tips can launch surface plasmons, which are then visible in the space-time maps along the fiber. When the surface waves reach the opposite tip of the fiber, they experience reflection and continue travelling in the opposite directions, forming a standing wave, or surface plasmon resonance, along the fiber. The standing wave results in periodic oscillations of the THz field visible in a time-domain waveform detected at the fiber center (Fig. 4(b)). The oscillation frequency is defined by the fiber length and the phase velocity, and the space-time maps reveal the oscillations' origin (Fig. 1(a)). The field evolution recorded along the fiber is similar to that observed in other THz plasmonic structures, and it helped unveiling how the excitation started and how it developed over time.

Optical Materials EXPRESS

4.2. Near-field probing of inter-resonator coupling and complex photonic states

The combination of spatial and temporal field sampling can also reveal the interplay between resonators in arrays and metasurfaces. The surface plasmon-mediated coupling modifies the response of a single isolated resonator into a collective far-field spectral response of a metasurface made of such resonators. However, the underlying coupling can only be inferred from far-field measurements, whereas near-field microscopy can visualize and help investigate the coupling experimentally.

Aperture-type near-field microscopy was recently used to map the field evolution in a complementary resonator metasurface (Fig. 5(a)), which contains an array of resonators 'cut out' in a continuous gold layer [26]. The experiment showed not only localized plasmon excitations, but also surface waves at the gold-air interface in spaces between resonators as well as beyond the array edges at distances over several hundreds of micrometers. The surface plasmons, excited at each individual resonator, travelled between resonators across the gold surface and interfered with the localized resonances, leading to modifications of the single resonator response. Although these surface plasmons can be recorded only at the top surface and the same phenomenon at the bottom (gold-substrate) is not accessible directly, the evolution of surface-confined fields between resonators offers an insight into the mechanisms of inter-resonator coupling [26,30].

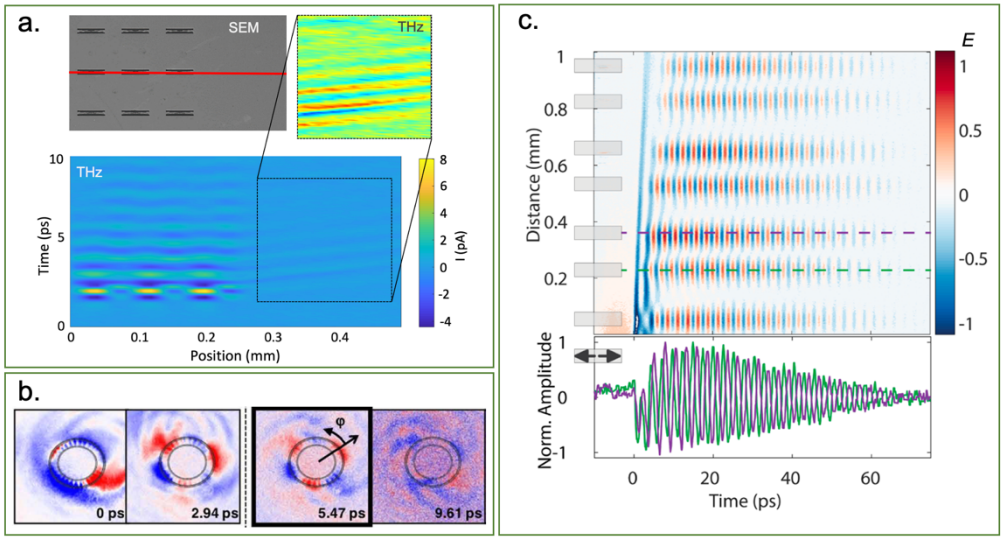

Fig. 5. a. Near-field mapping of surface plasmon waves propagating between complementary resonators in array: SEM image (*top*), THz near-field map recorded by aperture-type THz near-field microscopy (*bottom*), rescaled map of the detected field outside the array boundary where surface plasmon waves travel over 200 µm (adapted from [26] © 2020 Wiley-VCH). **b.** Near-field THz electro-optic mapping of specially designed corrugated metamaterial disks excited by a THz beam with orbital angular momentum. The sequence of maps shows a series of THz field 'snapshots' illustrating a localized spoof plasmon THz wave travelling along the outer circle in clockwise direction (adapted from [97]. © The Authors, some rights reserved; exclusive licensee AAAS. Distributed under a CC BY-NC 4.0 license. Reprinted with permission from AAAS). **c.** *Top panel:* Near-field mapping of BIC state with a space-time map of normalized THz field plotted at increasing distances from local excitation at −60 µm; *bottom panel:* harmonic out-of-phase oscillations of electric field in each dimer antenna pairs (adapted from [30], CC BY 4.0).

The possibility of field mapping over length scales of several resonators also enabled investigations of more complex photonic states. Recently, near-field THz detection via electro-optic

Optical Materials EXPRESS

sampling was used to visualize the transfer of orbital angular momentum from a THz vortex beam to specially designed corrugated metamaterial disks (Fig. 5(b)) [97]. Near-field observations in this study clearly showed the excitation of multipolar modes in the discs and their evolution in time. At the same time, the near-field approach also enabled characterization of the orbital angular momentum in the incident THz beams by mapping the spatial distribution of electric field.

To elucidate the internal working mechanisms of BIC states, van Hoof *et al.* demonstrated the use of THz micro-probes for both near-field detection as well as local THz excitation [30]. They excited a symmetry-protected BIC state in a metasurface comprising gold dimer resonators using a local THz source positioned in the near-field region of one of the dimers [30]. An electromagnetic wave propagating away from the point of excitation was imaged using a micro-probe scanned across the metasurface (Fig. 5(c)). The mapping of local fields in space and time enabled direct measurement of inter-resonator coupling in the symmetry-protected BIC state (Fig. 5(c)) [30]. It is worth emphasizing that the symmetry of the detected field distributions suppresses far-field radiation, making BIC metasurfaces challenging to characterize in the far-field.

4.3. Near-field probing of deeply subwavelength plasmon-polaritons

The large free-space wavelength of THz radiation constrains the minimal size of metallic and dielectric resonators to 10s of microns, limiting their potential for integration into future nanoscale devices. Some emerging materials however support light-matter excitations with wavelengths far shorter than the wavelength in free space – in the range of microns and 100s of nanometers [40,41,93,94], and therefore they provide a direct route to designing deeply subwavelength THz resonator elements.

s-SNOM has enabled detection and characterization of nanometric polaritons in the mid-IR – in particular, Dirac plasmons in 2D materials like graphene [93,94]. Their detection in the THz range however has proven more challenging. Only observation of 'acoustic' graphene plasmon modes has been reported so far [40,41], whereas detection of conventional graphene plasmons has proven difficult at THz frequencies, likely due to nanoscale disorder and charge carrier scattering resulting in plasmon decay rates faster than the period of the THz wave [46].

One of the most compelling alternatives to plasmons in graphene at THz frequencies are plasmons in topological insulators (TI), where strong spin-orbit coupling results in a metallic surface state – typically with Dirac dispersion – at the surface of an insulating material. Similar to graphene, this TI surface state can host strongly confined Dirac plasmons, but these are expected to emerge in the THz range due longer scattering times. Their elusive properties arising from the topological nature of the surface state, such as spin-polarization [98], remain the focus of current research (Fig. 6).

Very recently, THz s-SNOM measurements have been able to show plasmon-polaritons on TIs [45,46]. These observations were made possible due to the effect of plasmon launching by the tip of s-SNOM probe. Nanoscale-localized fields at the apex of an s-SNOM tip consist of a broad range of spatial frequencies (similar to the illustration in Fig. 2). The k-vectors that match that of propagating modes in the TI launch a propagating wave on the surface. When this process occurs at the edge of the sample, the propagating surface wave reflects from the edge and returns to the tip, where the wave is scattered by the tip and therefore can be detected by s-SNOM. In a near-field image, the surface plasmon wave forms an interference pattern near the edge (Fig. 6(a)). The wave properties, the plasmon wavelength and the decay length, therefore can be extracted directly from the s-SNOM-measured interference pattern (Fig. 6(b), c), and the plasmon-polariton dispersion can be mapped out by repeating these measurements for different frequencies of the THz source (Fig. 6(c)) [99].

While the Dirac surface states are promising for application in nanoscale resonators, other excitations in the TI exist in the THz range, including plasmons and phonons in the bulk as well as massive 2D electron gas formed by band bending at the surface [100]. These excitations result

Optical Materials EXPRESS

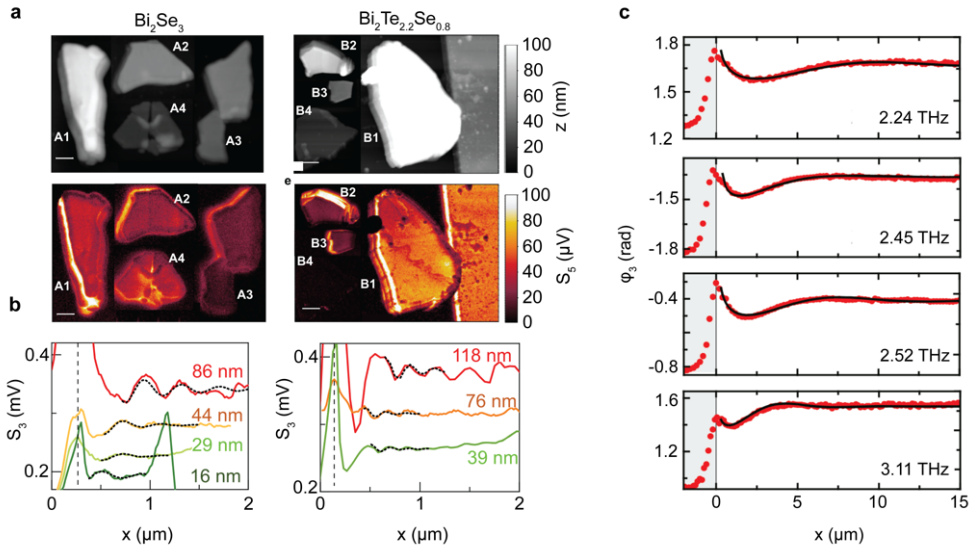

Fig. 6. Imaging propagating polaritons on topological insulators. **a.** Topography and scattered near-fields for several Bi_2Se_3 (left hand side) and $Bi_2Te_{2.2}Se_{0.8}$ (right hand side) flakes (adapted from [45], CC BY). **b.** Near-field line scans measured at 2 THz, showing the interference pattern formed by hybrid polaritons propagating in several Bi_2Se_3 (left hand side) and $Bi_2Te_{2.2}Se_{0.8}$ (right hand side) flakes shown in a. The dashed vertical line indicates the flake edge, and the thickness of each flake is indicated next to each linescan (adapted from [45], CC BY). **c.** Near-field line scans (phase of the scattered wave) sampled at multiple frequencies as function of the distance from the edge of a 60 nm thick Bi_2Se_3 layer, x, showing the interference pattern formed by hybrid polaritons. The vertical line at $x = 0\,\mu m$ and the grey shaded region mark the edge of Bi_2Se_3 (adapted from [46], CC BY).

in a complex dispersion relation consisting of several hybrid polariton excitations [45,46]. Many questions still remain, particularly the exact contribution of the topological surface state to the observed hybrid polaritons and the influence of the second TI surface state at the interface with the substrate. Nevertheless, the first near-field observations of THz plasmon-polaritons in TIs demonstrated the potential of THz-s-SNOM for exploring a diverse range of THz polaritonics and revealing the underlying physics. Furthermore, the use of near-field approaches will be essential in investigations of TIs patterned into resonators and metasurfaces.

5. Concluding remarks

In this review, we have outlined distinct insights provided by near-field THz microscopy in the continued development of THz metasurfaces. Each of the discussed near-field techniques can provide unique and complementary information needed for understanding the underlying electromagnetic field dynamics. They have revealed internal mechanisms operating in individual resonators and in metasurfaces, demonstrated detection of surface plasmon waves and localized resonances, enabled probing of vectorial components of the electric field and visualizing hybrid polariton excitations with sub-micron spatial resolution. Most of these physical phenomena are inaccessible for standard THz far-field spectroscopy and imaging.

THz near-field techniques still face serious technical challenges. First, sensitivity of THz near-field systems remains limited. By improving the efficiency of evanescent field detection in THz microscopes, it will be possible to capture smaller changes in evanescent fields and push spatial resolution beyond present limitations. Second, there currently exists a diverse range of

Optical Materials EXPRESS

approaches and systems with sometimes complex interpretations of measurements. While this diversity has benefited the establishing field of THz microscopy, beginning to standardize more rigorous methodologies for quantitative extraction of complex near-field signals and sample-probe interaction will help to both increase the accessibility of the field, as well as solidify the application potential of THz near-field microscopy in the eyes of the broader metasurface community. Finally, upcoming technological developments will undoubtedly widen the spectrum of applications, for example through enabling cryogenic temperatures, ultra-high vacuum conditions and the application of external magnetic fields. By opening doors for these unprecedented studies, THz near-field methods will help address a multitude of difficult, cutting-edge scientific questions, make unexpected discoveries, and develop novel resonator concepts exploiting emerging materials and novel concepts in photonic engineering.

Funding. Engineering and Physical Sciences Research Council (EP/L015277/1, EP/L015455/1, EP/P021859/1); Basic Energy Sciences.

Acknowledgments. This work was supported by EPSRC and by the U.S. Department of Energy, Office of Basic Energy Sciences, Division of Materials Sciences and Engineering.

Disclosures. The authors declare no conflicts of interest.

Data availability. No data were generated or analyzed in the presented research.

References

1. R. Ulbricht, E. Hendry, J. Shan, T. F. Heinz, and M. Bonn, "Carrier dynamics in semiconductors studied with time-resolved terahertz spectroscopy," Rev. Mod. Phys. **83**(2), 543–586 (2011).
2. J. Lloyd-Hughes and T.-I. Jeon, "A Review of the Terahertz Conductivity of Bulk and Nano-Materials," J. Infrared, Millimeter, Terahertz Waves **33**(9), 871–925 (2012).
3. J. A. Spies, J. Neu, U. T. Tayvah, M. D. Capobianco, B. Pattengale, S. Ostresh, and C. A. Schmuttenmaer, "Terahertz Spectroscopy of Emerging Materials," J. Phys. Chem. C **124**(41), 22335–22346 (2020).
4. N. I. Zheludev and Y. S. Kivshar, "From metamaterials to metadevices," Nat. Mater. **11**(11), 917–924 (2012).
5. A. V. Kildishev, A. Boltasseva, and V. M. Shalaev, "Planar Photonics with Metasurfaces," Science **339**(6125), 1232009 (2013).
6. H.-T. Chen, A. J. Taylor, and N. Yu, "A review of metasurfaces: physics and applications," Rep. Prog. Phys. **79**(7), 076401 (2016).
7. W. T. Chen, A. Y. Zhu, and F. Capasso, "Flat optics with dispersion-engineered metasurfaces," Nat. Rev. Mater. **5**(8), 604–620 (2020).
8. H.-T. Chen, W. J. Padilla, J. M. O. Zide, A. C. Gossard, A. J. Taylor, and R. D. Averitt, "Active terahertz metamaterial devices," Nature **444**(7119), 597–600 (2006).
9. W. J. Padilla, M. T. Aronsson, C. Highstrete, M. Lee, A. J. Taylor, and R. D. Averitt, "Electrically resonant terahertz metamaterials: Theoretical and experimental investigations," Phys. Rev. B **75**(4), 041102 (2007).
10. I. Al-Naib and W. Withayachumnankul, "Recent progress in terahertz metasurfaces," J. Infrared, Millimeter, Terahertz Waves **38**(9), 1067–1084 (2017).
11. B. Chen, X. Wang, W. Li, C. Li, Z. Wang, H. Guo, J. Wu, K. Fan, C. Zhang, Y. He, B. Jin, J. Chen, and P. Wu, "Electrically addressable integrated intelligent terahertz metasurface," Sci. Adv. **8**(41), eadd1296 (2022).
12. R. Degl'Innocenti, H. Lin, and M. Navarro-Cía, "Recent progress in terahertz metamaterial modulators," Nanophotonics **11**(8), 1485–1514 (2022).
13. S. Shen, X. Liu, Y. Shen, J. Qu, E. Pickwell-MacPherson, X. Wei, and Y. Sun, "Recent advances in the development of materials for terahertz metamaterial sensing," Adv. Opt. Mater. **10**(1), 2101008 (2022).
14. C. A. Curwen, J. L. Reno, and B. S. Williams, "Broadband continuous single-mode tuning of a short-cavity quantum-cascade VECSEL," Nat. Photonics **13**(12), 855–859 (2019).
15. S. Biasco, H. E. Beere, D. A. Ritchie, L. Li, A. G. Davies, E. H. Linfield, and M. S. Vitiello, "Frequency-tunable continuous-wave random lasers at terahertz frequencies," Light: Sci. Appl. **8**(1), 43 (2019).
16. Y. Zeng, U. Chattopadhyay, B. Zhu, B. Qiang, J. Li, Y. Jin, L. Li, A. G. Davies, E. H. Linfield, B. Zhang, Y. Chong, and Q. J. Wang, "Electrically pumped topological laser with valley edge modes," Nature **578**(7794), 246–250 (2020).
17. Y. Xu, J. Gu, Y. Gao, Q. Yang, W. Liu, Z. Yao, Q. Xu, J. Han, and W. Zhang, "Broadband achromatic terahertz metalens constituted by Si–SiO_2–Si hybrid meta-atoms," Adv. Funct. Mater. **33**(35), 2302821 (2023).
18. H. Zhao, B. Quan, X. Wang, C. Gu, J. Li, and Y. Zhang, "Demonstration of orbital angular momentum multiplexing and demultiplexing based on a metasurface in the terahertz band," ACS Photonics **5**(5), 1726–1732 (2018).
19. N. Yu and F. Capasso, "Flat optics with designer metasurfaces," Nat. Mater. **13**(2), 139–150 (2014).
20. K. M. Devi, S. Jana, and D. R. Chowdhury, "Topological edge states in an all-dielectric terahertz photonic crystal," Opt. Mater. Express **11**(8), 2445–2458 (2021).

Optical Materials EXPRESS

21. Y. Zhang, Y. Xu, C. Tian, Q. Xu, X. Zhang, Y. Li, X. Zhang, J. Han, and W. Zhang, "Terahertz spoof surface-plasmon-polariton subwavelength waveguide," Photonics Res. **6**(1), 18–23 (2018).
22. F. Pisani, D. Gacemi, A. Vasanelli, L. Li, A. G. Davies, E. Linfield, C. Sirtori, and Y. Todorov, "Electronic transport driven by collective light-matter coupled states in a quantum device," Nat. Commun. **14**(1), 3914 (2023).
23. O. Mitrofanov, F. Dominec, P. Kužel, J. L. Reno, I. Brener, U.-C. Chung, C. Elissalde, M. Maglione, and P. Mounaix, "Near-field probing of Mie resonances in single TiO_2 microspheres at terahertz frequencies," Opt. Express **22**(19), 23034 (2014).
24. I. Khromova, M. Navarro-Cía, I. Brener, J. L. Reno, A. Ponomarev, and O. Mitrofanov, "Dipolar resonances in conductive carbon micro-fibers probed by near-field terahertz spectroscopy," Appl. Phys. Lett. **107**(2), 021102 (2015).
25. O. Mitrofanov, Y. Todorov, D. Gacemi, A. Mottaghizadeh, C. Sirtori, I. Brener, and J. L. Reno, "Near-field spectroscopy and tuning of sub-surface modes in plasmonic terahertz resonators," Opt. Express **26**(6), 7437 (2018).
26. L. L. Hale, J. Keller, T. Siday, R. I. Hermans, J. Haase, J. L. Reno, I. Brener, G. Scalari, J. Faist, and O. Mitrofanov, "Noninvasive near-field spectroscopy of single subwavelength complementary resonators," Laser Photonics Rev. **14**(4), 1900254 (2020).
27. S. Rajabali, S. Markmann, E. Jöchl, M. Beck, C. A. Lehner, W. Wegscheider, J. Faist, and G. Scalari, "An ultrastrongly coupled single terahertz meta-atom," Nat. Commun. **13**(1), 2528 (2022).
28. M. Plankl, P. E. F. Junior, F. Mooshammer, T. Siday, M. Zizlsperger, F. Sandner, F. Schiegl, S. Maier, M. A. Huber, M. Gmitra, J. Fabian, J. L. Boland, T. L. Cocker, and R. Huber, "Subcycle contact-free nanoscopy of ultrafast interlayer transport in atomically thin heterostructures," Nat. Photonics **15**(8), 594–600 (2021).
29. H. R. Seren, J. Zhang, G. R. Keiser, S. J. Maddox, X. Zhao, K. Fan, S. R. Bank, X. Zhang, and R. D. Averitt, "Nonlinear terahertz devices utilizing semiconducting plasmonic metamaterials," Light: Sci. Appl. **5**(5), e16078 (2016).
30. N. J. J. van Hoof, D. R. Abujetas, S. E. T. ter Huurne, F. Verdelli, G. C. A. Timmermans, J. A. Sánchez-Gil, and J. G. Rivas, "Unveiling the symmetry protection of bound states in the continuum with terahertz near-field imaging," ACS Photonics **8**(10), 3010–3016 (2021).
31. E. A. Ash and G. Nicholls, "Super-resolution Aperture Scanning Microscope," Nature **237**(5357), 510–512 (1972).
32. F. Zenhausern, Y. Martin, and H. K. Wickramasinghe, "Scanning Interferometric Apertureless Microscopy: Optical Imaging at 10 Angstrom Resolution," Science **269**(5227), 1083–1085 (1995).
33. B. Knoll and F. Keilmann, "Near-field probing of vibrational absorption for chemical microscopy," Nature **399**(6732), 134–137 (1999).
34. A. I. Kuznetsov, A. E. Miroshnichenko, M. L. Brongersma, Y. S. Kivshar, and B. Luk'yanchuk, "Optically resonant dielectric nanostructures," Science **354**(6314), aag2472 (2016).
35. D. R. Smith, W. J. Padilla, D. C. Vier, S. C. Nemat-Nasser, and S. Schultz, "Composite medium with simultaneously negative permeability and permittivity," Phys. Rev. Lett. **84**(18), 4184–4187 (2000).
36. W. S. Lee, K. Kaltenecker, S. Nirantar, W. Withayachumnankul, M. Walther, M. Bhaskaran, B. M. Fischer, S. Sriram, and C. Fumeaux, "Terahertz near-field imaging of dielectric resonators," Opt. Express **25**(4), 3756–3764 (2017).
37. I. Khromova, P. Kužel, I. Brener, J. L. Reno, U. C. Seu, C. Elissalde, M. Maglione, P. Mounaix, and O. Mitrofanov, "Splitting of magnetic dipole modes in anisotropic TiO_2 micro-spheres," Laser Photonics Rev. **10**(4), 681–687 (2016).
38. O. Mitrofanov, W. Yu, R. J. Thompson, Y. Jiang, I. Brener, W. Pan, C. Berger, W. A. de Heer, and Z. Jiang, "Probing terahertz surface plasmon waves in graphene structures," Appl. Phys. Lett. **103**(11), 111105 (2013).
39. O. Mitrofanov, W. Yu, R. J. Thompson, Y. Jiang, Z. J. Greenberg, J. Palmer, I. Brener, W. Pan, C. Berger, W. A. de Heer, and Z. Jiang, "Terahertz near-field imaging of surface plasmon waves in graphene structures," Solid State Commun. **224**, 47–52 (2015).
40. P. Alonso-González, A. Y. Nikitin, Y. Gao, A. Woessner, M. B. Lundeberg, A. Principi, N. Forcellini, W. Yan, S. Vélez, J. Andreas, K. Huber, T. Watanabe, F. Taniguchi, L. E. Casanova, M. Hueso, J. Polini, F. H. L. Hone, R. Koppens, and Hillenbrand, "Acoustic terahertz graphene plasmons revealed by photocurrent nanoscopy," Nat. Nanotechnol. **12**(1), 31–35 (2017).
41. M. B. Lundeberg, Y. Gao, R. Asgari, C. Tan, B. V. Duppen, M. Autore, P. Alonso-González, A. Woessner, K. Watanabe, T. Taniguchi, R. Hillenbrand, J. Hone, M. Polini, and F. H. L. Koppens, "Tuning quantum nonlocal effects in graphene plasmonics," Science **357**(6347), 187–191 (2017).
42. H. Park, S. Jeong, C. Seo, H. Park, D. Oh, J.-E. Shim, J. Lee, T. Ha, H.-D. Kim, S. Baek, B. Min, and T.-T. Kim, "Electrically tunable THz graphene metasurface wave retarders," Nanophotonics **12**(13), 2553–2562 (2023).
43. P. Di Pietro, M. Ortolani, O. Limaj, A. Di Gaspare, V. Giliberti, F. Giorgianni, M. Brahlek, N. Bansal, N. Koirala, S. Oh, P. Calvani, and S. Lupi, "Observation of Dirac plasmons in a topological insulator," Nat. Nanotechnol. **8**(8), 556–560 (2013).
44. T. P. Ginley and S. Law, "Coupled Dirac Plasmons in Topological Insulators," Adv. Opt. Mater. **6**(13), 1800113 (2018).
45. E. A. A. Pogna, L. Viti, A. Politano, M. Brambilla, G. Scamarcio, and M. S. Vitiello, "Mapping propagation of collective modes in Bi_2Se_3 and $Bi_2Te_{2.2}Se_{0.8}$ topological insulators by near-field terahertz nanoscopy," Nat. Commun. **12**(1), 6672 (2021).

Optical Materials EXPRESS

46. S. Chen, A. Bylinkin, Z. Wang, M. Schnell, G. Chandan, P. Li, A. Y. Nikitin, S. Law, and R. Hillenbrand, "Real-space nanoimaging of THz polaritons in the topological insulator Bi_2Se_3," Nat. Commun. **13**(1), 1374 (2022).
47. L. L. Hale, Z. Wang, C. T. Harris, I. Brener, S. Law, and O. Mitrofanov, "Near-field spectroscopy of Dirac plasmons in Bi_2Se_3 ribbon arrays," APL Photonics **8**(5), 051304 (2023).
48. R. H. J. Kim, C. Huang, Y. Luan, L.-L. Wang, Z. Liu, J.-M. Park, L. Luo, P. M. Lozano, G. Gu, D. Turan, N. T. Yardimci, M. Jarrahi, I. E. Perakis, Z. Fei, Q. Li, and J. Wang, "Terahertz Nano-Imaging of Electronic Strip Heterogeneity in a Dirac Semimetal," ACS Photonics **8**(7), 1873–1880 (2021).
49. Q. Lu, A. T. Bollinger, X. He, R. Sundling, I. Bozovic, and A. Gozar, "Surface Josephson plasma waves in a high-temperature superconductor," npj Quantum Mater. **5**(1), 69 (2020).
50. Z. Sun, M. M. Fogler, D. N. Basov, and A. J. Millis, "Collective modes and terahertz near-field response of superconductors," Phys. Rev. Res. **2**(2), 023413 (2020).
51. O. Mitrofanov, C. C. Renaud, and A. J. Seeds, "Terahertz probe for spectroscopy of sub-wavelength objects," Opt. Express **20**(6), 6197–6202 (2012).
52. B. B. Hu and M. C. Nuss, "Imaging with terahertz waves," Opt. Lett. **20**(16), 1716–1718 (1995).
53. Q. Wu and X. -C. Zhang, "Ultrafast electro-optic field sensors," Appl. Phys. Lett. **68**(12), 1604–1606 (1996).
54. S. Hunsche, M. Koch, I. Brener, and M. C. Nuss, "THz near-field imaging," Opt. Commun. **150**(1-6), 22–26 (1998).
55. O. Mitrofanov, M. Lee, J. W. P. Hsu, L. N. Pfeiffer, K. W. West, J. D. Wynn, and J. F. Federici, "Terahertz pulse propagation through small apertures," Appl. Phys. Lett. **79**(7), 907–909 (2001).
56. N. C. J. van der Valk and P. C. M. Planken, "Electro-optic detection of subwavelength terahertz spot sizes in the near field of a metal tip," Appl. Phys. Lett. **81**(9), 1558–1560 (2002).
57. H.-T. Chen, R. Kersting, and G. C. Cho, "Terahertz imaging with nanometer resolution," Appl. Phys. Lett. **83**(15), 3009–3011 (2003).
58. A. J. Huber, F. Keilmann, J. Wittborn, J. Aizpurua, and R. Hillenbrand, "Terahertz Near-Field Nanoscopy of Mobile Carriers in Single Semiconductor Nanodevices," Nano Lett. **8**(11), 3766–3770 (2008).
59. C. Maissen, S. Chen, E. Nikulina, A. Govyadinov, and R. Hillenbrand, "Probes for Ultrasensitive THz Nanoscopy," ACS Photonics **6**(5), 1279–1288 (2019).
60. A. Leitenstorfer, A. S. Moskalenko, T. Kampfrath, J. Kono, E. Castro-Camus, K. Peng, N. Qureshi, D. Turchinovich, K. Tanaka, and A. G. Markelz, "The 2023 terahertz science and technology roadmap," J. Phys. D: Appl. Phys. **56**(22), 223001 (2023).
61. O. Mitrofanov, M. Lee, J. W. P. Hsu, I. Brener, R. Harel, J. F. Federici, J. D. Wynn, L. N. Pfeiffer, and K. W. West, "Collection-Mode Near-Field Imaging With 0.5-THz Pulses," IEEE J. Sel. Top. Quantum Electron. **7**(4), 600–607 (2001).
62. A. J. Macfaden, J. L. Reno, I. Brener, and O. Mitrofanov, "3 μm aperture probes for near-field terahertz transmission microscopy," Appl. Phys. Lett. **104**(1), 011110 (2014).
63. O. Mitrofanov, I. Khromova, T. Siday, R. J. Thompson, A. N. Ponomarev, I. Brener, and J. L. Reno, "Near-Field Spectroscopy and Imaging of Subwavelength Plasmonic Terahertz Resonators," IEEE Trans. Terahertz Sci. Technol. **6**(3), 382–388 (2016).
64. N. C. J. van der Valk and P. C. M. Planken, "Measurement of THz Spot Sizes with a λ/200 Diameter in the Near-Field of a Metal Tip," J. Biol. Phys. **29**(2/3), 239–245 (2003).
65. M. A. Seo, A. J. L. Adam, J. H. Kang, J. W. Lee, K. J. Ahn, Q. H. Park, P. C. M. Planken, and D. S. Kim, "Near field imaging of terahertz focusing onto rectangular apertures," Opt. Express **16**(25), 20484–20489 (2008).
66. O. Mitrofanov, "Tetrahertz near-field electro-optic probe based on a microresonator," Appl. Phys. Lett. **88**(9), 091118 (2006).
67. F. Blanchard and K. Tanaka, "Improving time and space resolution in electro-optic sampling for near-field terahertz imaging," Opt. Lett. **41**(20), 4645 (2016).
68. A. Bhattacharya and J. G. Rivas, "Full vectorial mapping of the complex electric near-fields of THz resonators," APL Photonics **1**(8), 086103 (2016).
69. T. L. Cocker, V. Jelic, R. Hillenbrand, and F. A. Hegmann, "Nanoscale terahertz scanning probe microscopy," Nat. Photonics **15**(8), 558–569 (2021).
70. X. Chen, D. Hu, R. Mescall, G. You, D. N. Basov, Q. Dai, and M. Liu, "Modern scattering-type scanning near-field optical microscopy for advanced material research," Adv. Mater. **31**(24), 1804774 (2019).
71. K. Wang, D. M. Mittleman, N. C. J. van der Valk, and P. C. M. Planken, "Antenna effects in terahertz apertureless near-field optical microscopy," Appl. Phys. Lett. **85**(14), 2715–2717 (2004).
72. S. Mastel, M. B. Lundeberg, P. Alonso-González, Y. Gao, K. Watanabe, T. Taniguchi, J. Hone, F. H. L. Koppens, A. Y. Nikitin, and R. Hillenbrand, "Terahertz Nanofocusing with Cantilevered Terahertz-Resonant Antenna Tips," Nano Lett. **17**(11), 6526–6533 (2017).
73. T. Siday, M. Natrella, J. Wu, H. Liu, and O. Mitrofanov, "Resonant terahertz probes for near-field scattering microscopy," Opt. Express **25**(22), 27874 (2017).
74. M. Dapolito, X. Chen, C. Li, M. Tsuneto, S. Zhang, X. Du, M. Liu, and A. Gozar, "Scattering-type scanning near-field optical microscopy with Akiyama piezo-probes," Appl. Phys. Lett. **120**(1), 013104 (2022).
75. N. Sulollari, J. Keeley, S. Park, P. Rubino, A. D. Burnett, L. Li, M. C. Rosamond, E. H. Linfield, A. G. Davies, J. E. Cunningham, and P. Dean, "Coherent terahertz microscopy of modal field distributions in micro-resonators," APL Photonics **6**(6), 066104 (2021).

Optical Materials EXPRESS

76. R. Jing, Y. Shao, Z. Fei, C. F. B. Lo, R. A. Vitalone, F. L. Ruta, J. Staunton, W. J.-C. Zheng, A. S. Mcleod, Z. Sun, B. Jiang, X. Chen, M. M. Fogler, A. J. Millis, M. Liu, D. H. Cobden, X. Xu, and D. N. Basov, "Terahertz response of monolayer and few-layer WTe_2 at the nanoscale," Nat. Commun. **12**(1), 5594 (2021).
77. J. Zhang, X. Chen, S. Mills, T. Ciavatti, Z. Yao, R. Mescall, H. Hu, V. Semenenko, Z. Fei, H. Li, V. Perebeinos, H. Tao, Q. Dai, X. Du, and M. Liu, "Terahertz Nanoimaging of Graphene," ACS Photonics **5**(7), 2645–2651 (2018).
78. P. Klarskov, H. Kim, V. L. Colvin, and D. M. Mittleman, "Nanoscale laser terahertz emission microscopy," ACS Photonics **4**(11), 2676–2680 (2017).
79. T. Siday, F. Sandner, S. Brem, M. Zizlsperger, R. Perea-Causin, F. Schiegl, S. Nerreter, M. Plankl, P. Merkl, F. Mooshammer, M. A. Huber, E. Malic, and R. Huber, "Ultrafast Nanoscopy of High-Density Exciton Phases in WSe_2," Nano Lett. **22**(6), 2561–2568 (2022).
80. F. Mooshammer, M. Plankl, T. Siday, M. Zizlsperger, F. Sandner, R. Vitalone, R. Jing, M. A. Huber, D. N. Basov, and R. Huber, "Quantitative terahertz emission nanoscopy with multiresonant near-field probes," Opt. Lett. **46**(15), 3572–3575 (2021).
81. T. Siday, L. L. Hale, R. I. Hermans, and O. Mitrofanov, "Resonance-Enhanced Terahertz Nanoscopy Probes," ACS Photonics **7**(3), 596–601 (2020).
82. O. Mitrofanov, Z. Han, F. Ding, S. I. Bozhevolnyi, I. Brener, and J. L. Reno, "Detection of internal fields in double-metal terahertz resonators," Appl. Phys. Lett. **110**(6), 061109 (2017).
83. G. Valušis, A. Lisauskas, H. Yuan, W. Knap, and H. G. Roskos, "Roadmap of Terahertz Imaging 2021," Sensors **21**(12), 4092 (2021).
84. R. Mueckstein, C. Graham, C. C. Renaud, A. J. Seeds, J. A. Harrington, and O. Mitrofanov, "Imaging and analysis of THz surface plasmon polariton waves with the integrated sub-wavelength aperture probe," J. Infrared, Millimeter, Terahertz Waves **32**(8-9), 1031–1042 (2011).
85. L. Yuezhen, L. L. Hale, A. Zaman, S. Addamane, I. Brener, O. Mitrofanov, and R. Degl'Innocenti, "Near-field spectroscopy of individual asymmetric split-ring Terahertz resonators," ACS Photonics (in press).
86. M. C. Giordano, L. Viti, O. Mitrofanov, and M. S. Vitiello, "Phase-sensitive terahertz imaging using room-temperature near-field nanodetectors," Optica **5**(5), 651–657 (2018).
87. O. Mitrofanov, L. Viti, E. Dardanis, M. C. Giordano, D. Ercolani, A. Politano, L. Sorba, and M. S. Vitiello, "Near-field terahertz probes with room-temperature nanodetectors for subwavelength resolution imaging," Sci. Rep. **7**(1), 44240 (2017).
88. J. Grzyb, B. Heinemann, and U. R. Pfeiffer, "Solid-state terahertz superresolution imaging device in 130-nm SiGe BiCMOS technology," IEEE Trans. Microwave Theory Tech. **65**(11), 4357–4372 (2017).
89. Y. Kawano and K. Ishibashi, "An on-chip near-field terahertz probe and detector," Nat. Photonics **2**(10), 618–621 (2008).
90. R. Degl'Innocenti, R. Wallis, B. Wei, L. Xiao, S. J. Kindness, O. Mitrofanov, P. Braeuninger-Weimer, S. Hofmann, H. E. Beere, and D. A. Ritchie, "Terahertz nanoscopy of plasmonic resonances with a quantum cascade laser," ACS Photonics **4**(9), 2150–2157 (2017).
91. L. Thomas, T. Hannotte, C. N. Santos, B. Walter, M. Lavancier, S. Eliet, M. Faucher, J.-F. Lampin, and R. Peretti, "Imaging of THz photonic modes by scattering scanning near-field optical microscopy," ACS Appl. Mater. Interfaces **14**(28), 32608–32617 (2022).
92. V. Pushkarev, H. Němec, V. C. Paingad, J. Maňák, V. Jurka, V. Novák, T. Ostatnický, and P. Kužel, "Charge transport in single-crystalline gaas nanobars: impact of band bending revealed by terahertz spectroscopy," Adv. Funct. Mater. **32**(5), 2107403 (2022).
93. J. Chen, M. Badioli, P. Alonso-González, S. Thongrattanasiri, F. Huth, J. Osmond, M. Spasenović, A. Centeno, A. Pesquera, P. Godignon, A. Z. Elorza, N. Camara, F. J. G. de Abajo, R. Hillenbrand, and F. H. L. Koppens, "Optical nano-imaging of gate-tunable graphene plasmons," Nature **487**(7405), 77–81 (2012).
94. Z. Fei, A. S. Rodin, G. O. Andreev, W. Bao, A. S. McLeod, M. Wagner, L. M. Zhang, Z. Zhao, M. Thiemens, G. Dominguez, M. M. Fogler, A. H. C. Neto, C. N. Lau, F. Keilmann, and D. N. Basov, "Gate-tuning of graphene plasmons revealed by infrared nano-imaging," Nature **487**(7405), 82–85 (2012).
95. A. Cvitkovic, N. Ocelic, and R. Hillenbrand, "Analytical model for quantitative prediction of material contrasts in scattering-type near-field optical microscopy," Opt. Express **15**(14), 8550–8565 (2007).
96. B. Hauer, A. P. Engelhardt, and T. Taubner, "Quasi-analytical model for scattering infrared near-field microscopy on layered systems," Opt. Express **20**(12), 13173 (2012).
97. T. Arikawa, T. Hiraoka, S. Morimoto, F. Blanchard, S. Tani, T. Tanaka, K. Sakai, H. Kitajima, K. Sasaki, and K. Tanaka, "Transfer of orbital angular momentum of light to plasmonic excitations in metamaterials," Sci. Adv. **6**(24), eaay1977 (2020).
98. H.-H. Kung, S. Maiti, X. Wang, S.-W. Cheong, D. L. Maslov, and G. Blumberg, "Chiral spin mode on the surface of a topological insulator," Phys. Rev. Lett. **119**(13), 136802 (2017).
99. G. X. Ni, L. Wang, M. D. Goldflam, M. Wagner, Z. Fei, A. S. McLeod, M. K. Liu, F. Keilmann, B. Özyilmaz, A. H. C. Neto, J. Hone, M. M. Fogler, and D. N. Basov, "Ultrafast optical switching of infrared plasmon polaritons in high-mobility graphene," Nat. Photonics **10**(4), 244–247 (2016).
100. F. Mooshammer, F. Sandner, M. A. Huber, M. Zizlsperger, H. Weigand, M. Plankl, C. Weyrich, M. Lanius, J. Kampmeier, G. Mussler, D. Grützmacher, J. L. Boland, T. L. Cocker, and R. Huber, "Nanoscale near-field tomography of surface states on $(Bi_{0.5}Sb_{0.5})_2Te_3$," Nano Lett. **18**(12), 7515–7523 (2018).